The Meteoritical Society

Meteoritics & Planetary Science 43, Nr 6, 1–crossref to last page (2008)
Abstract available online at http://meteoritics.org

Physical properties of meteorites—Applications in space missions to asteroids

T. KOHOUT[1, 2, 3*], G. KLETETSCHKA[3, 4, 5], T. ELBRA[1], T. ADACHI[4, 5], V. MIKULA[4, 5], L. J. PESONEN[1], P. SCHNABL[2, 3], and S. SLECHTA[2, 3]

[1]Department of Physics, University of Helsinki, P. O. Box 64, 00014, Helsinki, Finland
[2]Department of Applied Geophysics, Charles University, Prague, Czech Republic
[3]Institute of Geology, Academy of Sciences, Prague, Czech Republic
[4]Department of Physics, Catholic University of America, Washington, D.C., USA
[5]GSFC/NASA; Code 691, Greenbelt, Maryland, USA
[*]Corresponding author. E-mail: tomas.kohout@helsinki.fi

(Received 06 January 2008; revision accepted 15 June 2008)

Abstract–Based on reflectance spectroscopy and chemical/mineralogical remote sensing methods, it is generally assumed that asteroids are parent bodies for most meteorites reaching the Earth. However, more detailed observations indicate that differences exist in composition between asteroids and meteorites resulting in difficulties when searching for meteorite-asteroid match.

We show that among other physical parameters the magnetic susceptibility of an asteroid can be determined remotely from the magnetic induction by solar wind using an orbiting spacecraft or directly using the AC coil on the lander, or it can be measured in samples returned to the laboratory. The shape corrected value of the true magnetic susceptibility of an asteroid can be compared to those of meteorites in the existing database, allowing closer match between asteroids and meteorites. The database of physical properties contains over 700 samples and was recently enlarged with measurements of meteorites in European museums using mobile laboratory facility.

INTRODUCTION

The objective of asteroid and comet investigation is the characterization and classification of these bodies using remote data acquisition systems. It is generally assumed that asteroids are parent bodies for most meteorites reaching the Earth (Wasson and Wetherill 1979; Feirberg et al. 1982). The reflectance spectroscopy of asteroids proved to be a powerful tool in characterization of the asteroid composition and classification. The extended taxonomy (Tholen 1984; modified by Bus and Binzel 2002) defines 26 classes of the asteroid reflectance spectra. Three major groupings (S, C, and X complexes) show spectral similarities to the major meteorite groups. The composition of the S-class asteroids is similar to the silicate-rich ordinary chondrite group, the C-class contains asteroids that are rich in carbonaceous material similar to that of carbonaceous chondrite group, and X-class contains various asteroid types mostly rich in metallic component. However, when analyzing the whole spectral curve, the exact match between asteroids and meteorites is not found due to differences in their spectral patterns.

Thus, other remote sensing methods are applied during asteroid reconnaissance in order to improve the knowledge of the asteroid chemical and mineralogical composition and to determine possible meteorite equivalents to the asteroid compositions. We show that the physical properties of asteroids and meteorites—mainly the magnetic susceptibility and density—can be applied along with the chemical and mineralogical methods in building the link between meteorites and asteroids.

INSTRUMENTS AND METHODS

The meteorites represent a valuable, rare material, and it is difficult to bring meteorites directly to the laboratory for scientific studies. Thus, the mobile laboratory facility including portable instrumentation was assembled at Division of Geophysics, University of Helsinki, to perform the research tour over the museums and collections in Europe and to measure the physical properties of meteorites using harmless, non-destructive methods.

During the meteorite research tour, the measurements of bulk physical parameters (magnetic susceptibility, bulk and grain density, and porosity) of meteorites were performed. Due to the rare nature of meteorites, only harmless, non-destructive methods were applied.

The Hämäläinen TH-1 portable susceptibility meter with a large (12 cm) coil was used for susceptibility measurements of bulk samples and was cross-calibrated with the laboratory's RISTO 5 and Agico KLY-3 susceptibility meters.

To determine the meteorite bulk and grain density as well as porosity the bulk and grain volume and mass must be measured. For bulk volume measurements, the chemically inert tiny glass beads (20–50 μm) were used to replace liquids used in traditional Archimedean method. The precision of the glass beads method is ±0.1 cm^3. The mass was determined using digital OHAUS balances. The balances were always calibrated prior the measurements using mass standards.

The grain volume was measured by Notari portable air pycnometer working at low pressures. The advantage of this instrument is that it does not require any supply of gas and thus is easy to transport. The precision of the pycnometer is ±0.1 cm^3.

The instruments can be easily fitted in a small van serving as a mobile meteorite laboratory (Kohout et al. 2006). This approach enables to perform the meteorite physical properties measurements using non-destructive methods directly in the meteorite collections under the supervision of the curator.

Figures 1 and 2 compare the data obtained in the museums using mobile meteorite laboratory (colored symbols) with the older data obtained using fixed laboratory instrumentation (grey symbols). The good agreement between those two data sets proves a good cross-calibration between the portable and laboratory instrumentations.

MAGNETIC SUSCEPTIBILITY OF STONY METEORITES

Magnetic susceptibility of various meteorites has been systematically studied by Kukkonen and Pesonen (1983), Terho et al. (1993a, 1993b), Rochette et al. (2001, 2003, 2008), and Kohout et al. (2006). The results of these studies indicate that the magnetic susceptibility of various meteorite clans and groups occupy characteristic values with quite uniform distribution (Fig. 1). According to those studies, the lowest susceptibility is occupied by SNC (10–100 10^{-8} m^3/kg) and HED (10–1000 10^{-8} m^3/kg) achondrites. Aubrites have also low-susceptibility values (400–3000 10^{-8} m^3/kg). Chondrite clan has higher susceptibilities in the range of 4000–80,000 10^{-8} m^3/kg (with the exception of R chondrites that occupy the range of 100–160 10^{-8} m^3/kg), and stony-irons and irons occupy the highest susceptibility range (100,000–2,000,000 10^{-8} m^3/kg). However, it is difficult to measure the true magnetic susceptibility of stony-irons and irons due to the shape effect (see section The Role of Shape and Demagnetization Factor), and thus the values contain high level of uncertainty.

The iron content of undifferentiated meteorites is both within the silicates and in the form of fine magnetic grains. Magnetic properties of ordinary chondrite clan (Wasilewski et al. 2002) are mostly related to Fe-Ni compounds, namely α-kamacite (<7% Ni), γ-taenite (>7% Ni), and γ-tetrataenite (43–52% Ni) capable of carrying remanent magnetization (Morden and Collinson 1992; Wasilewski 1988). The susceptibility of the ordinary chondrites (Fig. 2) is directly related to the amount of metal (FeNi) fraction in non-oxidized form. The lowest susceptibility values occupy the LL-chondrite group with the range of approximately 300–4000 10^{-8} m^3/kg followed by the L-chondrite group (4000–14,000 10^{-8} m^3/kg), and the H chondrite group (14,000–46,000 10^{-8} m^3/kg). The susceptibility of enstatite chondrite clan falls mostly in the range of 46000–80000 10^{-8} m^3/kg. Ureilites occupy similar susceptibility range (6000–15000 10^{-8} m^3/kg) as L-type chondrites.

The magneto-mineralogy of the carbonaceous chondrite clan (Rochette et al. 2008) is more complicated containing not only the FeNi, but also oxides, sulfides, and carbides. The CM, CV, and C2 groups occupy roughly the range of 400–4000 10^{-8} m^3/kg, while the CO3, CK, and CI groups fall mostly in the range of 2500–6300 10^{-8} m^3/kg. The C3-4 groups are characterized by susceptibilities in range of 3100–10,000 10^{-8} m^3/kg. The CR group has values around 10,000 10^{-8} m^3/kg. The highest susceptibility values among carbonaceous chondrites (comparable with those of the enstatite chondrite clan) belong to the CH group with the range of 16,000–63,000 10^{-8} m^3/kg. The magnetic susceptibilities of various carbonaceous chondrite groups overlap and are similar to those of ordinary chondrites. However, when compared with ordinary chondrites, the carbonaceous chondrites have, in general, lower bulk and grain densities (Consolmagno and Britt 1998; Britt and Consolmagno 2003; Wilkinson et al. 2003).

THE FINNISH DATABASE OF PHYSICAL PROPERTIES OF METEORITES

The research work of Kukkonen and Pesonen 1983; Terho et al. 1993a, 1993b and Kohout et al. 2006 has been has been merged in a form of database counting measurements of more than 700 individual meteorite samples from European meteorite collections and is continuously expanded. The database contains measurements of physical parameters including bulk (volume normalized) and mass susceptibility, bulk and grain density, porosity, NRM (Natural Remanent Magnetization), Q-value (Königsberger ratio), various hysteresis parameters and magnetic paleointensity estimates.

In Table 1 we present new unpublished mass normalized as well as volume normalized shape corrected magnetic susceptibility values, bulk and grain densities and porosities of meteorite samples obtained using the mobile laboratory (colored symbols in Figs. 1 and 2).

THE ROLE OF THE SHAPE AND DEMAGNETIZATION FACTOR

The magnetic susceptibility κ of the body determined in the ambient magnetic field B is influenced by the shape and

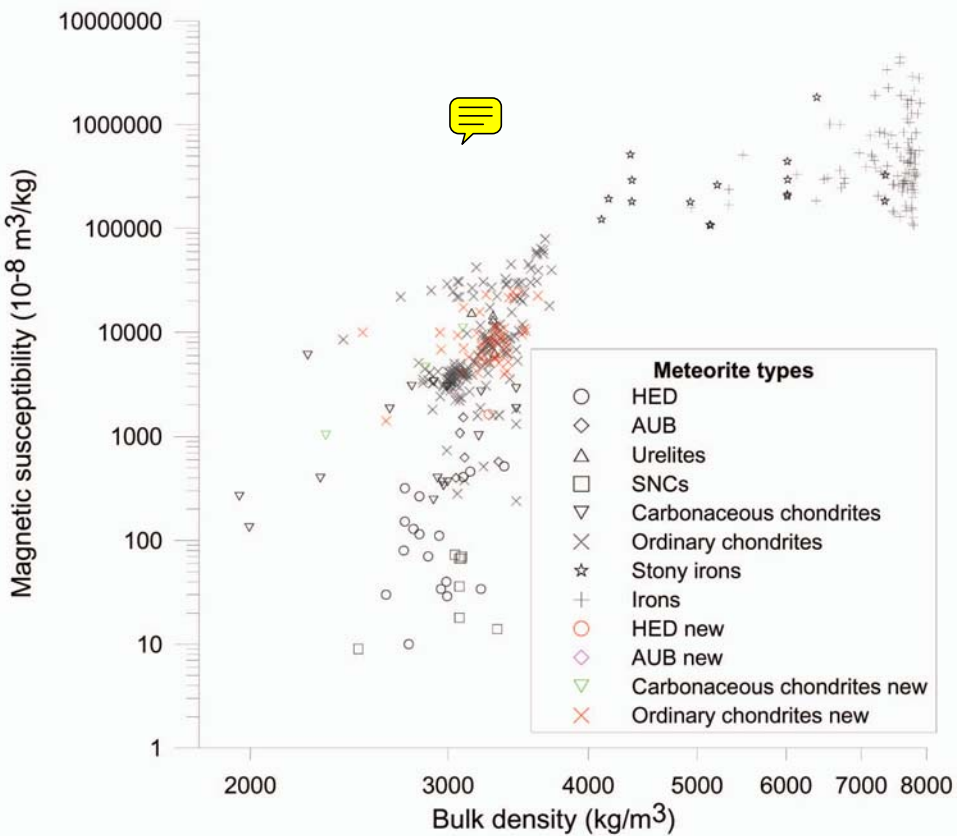

Fig. 1. Magnetic susceptibility versus bulk density of various meteorite clans. The lowest magnetic susceptibility values are characteristic to achondrites, followed by the chondrites, stony-irons and irons. The carbonaceous chondrite clan shows lowest bulk densities followed by other stony meteorites, stony-irons and iron meteorites. The grey symbols show older data obtained in laboratory while the colored symbols show new data measured directly in the museums using portable instruments. Only unweathered falls are displayed.

dimensions of the body. Thus the measured (apparent) magnetic susceptibility κ_A should be corrected for this shape effect to obtain the shape-independent true susceptibility κ_T. As a shape-independent parameter, the true susceptibility can be used as a comparative parameter between meteorites and asteroids.

The relation between the true and apparent volume susceptibility is characterized by Equations 1 and 2:

$$\kappa_T = \frac{\kappa_A}{1 - N\kappa_A} \quad (1)$$

or

$$\kappa_A = \frac{\kappa_T}{1 + N\kappa_T} \quad (2)$$

where N is the demagnetizing factor. The demagnetizing factor is depending on the shape of the object and direction along which the magnetic susceptibility is determined. For ellipsoid-shaped bodies, the demagnetization factor can be calculated along the ellipsoid axes using the approach of Osborn (1945).

In Table 2 the shape effect has been determined for the rotational ellipsoids with various a to b, c axis ratios and for the susceptibilities ranging from 500 to 500,000 10^{-8} m^3/kg (0.016 to 16 SI, assuming density of 3200 kg/m^3). It is apparent that at the susceptibility values ~0.1 SI, the difference between κ_A and κ_T for elongated objects can reach more than 10%. At even higher susceptibility values this difference is more pronounced, and for values $\kappa_T >> 1$ SI Equation 2 reaches the form of Equation 3:

$$\kappa_A \approx \frac{1}{N}. \quad (3)$$

This condition is met for iron and stony-iron meteorites and thus the apparent susceptibility κ_A is strongly controlled by the shape of the body, and the true susceptibility value κ_T contains large uncertainty resulting in large scatter of the true susceptibility values (see Fig. 1).

All meteorite susceptibility values presented in Figs. 1 and 2 are corrected for the shape of the sample.

DETERMINATION OF ASTEROIDAL MAGNETIC SUSCEPTIBILITY

Knowledge of asteroidal magnetic susceptibility could help identify the metallic nature of an asteroid's interior

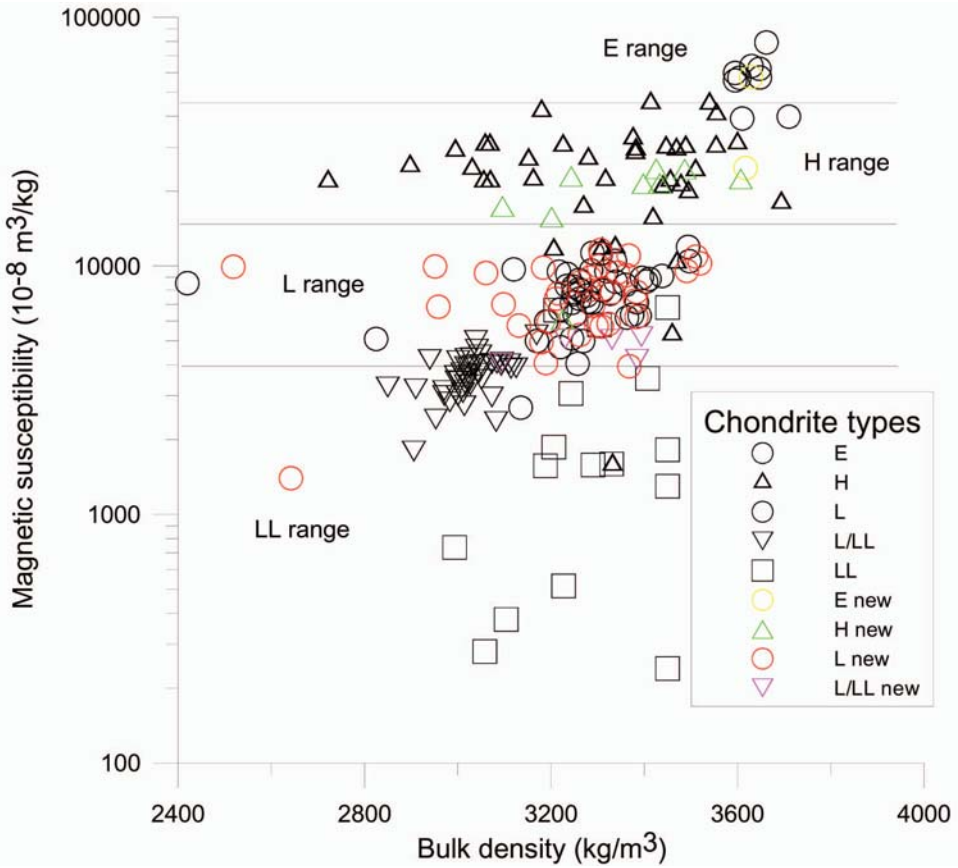

Fig. 2. Magnetic susceptibility versus bulk density of various ordinary chondrite groups and of enstatite chondrite clan. The magnetic susceptibility increases from LL chondrites to L, H and E chondrites. The grey symbols show older data obtained in laboratory while the colored symbols show new data measured directly in the museums using portable instruments. Only unweathered falls are displayed.

without direct access. However, the determination of this parameter is not an easy task. Magnetic susceptibility of the asteroid may be detected in three ways with various levels of uncertainty:

1. Passively from an induced magnetization by interplanetary magnetic field (IMF).
2. Actively using a surface probe (AC coil) attached to a lander.
3. Directly in a sample returned from an asteroid.

Remote Determination of the Asteroidal Magnetic Susceptibility from Induced Magnetization by Interplanetary Magnetic Field

The interplanetary magnetic field (IMF) is carried through the solar system in the solar wind. When encountering the asteroid, the IMF gets disturbed. The level of this interaction depends on the magnetic properties of the asteroid. The asteroids with low remanent magnetization and low magnetic susceptibility will cause minor distortion, while the asteroids with high remanent magnetization and/or high magnetic susceptibility can cause high disturbances in the IMF.

Those interactions can be measured using an orbiting spacecraft equipped with a magnetometer. In the case when significant interactions between asteroid and IMF have been detected, the first task is to separate the interactions due to the remanent magnetization from those due to the induced effect. Only the induced magnetization contains the information about the magnetic susceptibility. The basic criteria used to separate the remanent and induced magnetization are the facts that remanent magnetization of an asteroid has a stable value and direction and thus rotates with the asteroid, while the induced (by the IMF) magnetization has always the direction of the IMF and its magnitude correlates positively with the magnitude of the IMF (and with the magnetic susceptibility of the asteroid). The remanent magnetization of an asteroid can be also easily determined in the periods of low IMF magnitudes when the induced effects are negligible.

Once the remanent magnetic field of an asteroid is well determined or it is determined that the asteroid has negligible remanence, the induced magnetic field during the periods of the high IMF magnitudes can be used to determine the magnetic susceptibility (Kletetschka et al., unpublished data).

The separation of the induced magnetic measurements

Table 1. New mass-normalized (KM) and volume-normalized (KV) shape-corrected magnetic susceptibility values, bulk (BD) and grain (GD) densities, and porosities (P) of meteorite samples obtained using the mobile laboratory.

Meteorite	Collections	Type	Fall/find (date)	Mass (g)	BD (kg/m^3)	GD (kg/m^3)	P (%)	KM (Osb) (10^{-8} m^3/kg)	KV (Osb) (10^{-6} SI)
Juvinas	IGGL	AEUC	FA 15/06/1821	8.26	2503	3177	21		
Andrioniškio	VUV	AEUC	FA 1929	14.34	2988	3259	8		
Bereba	IGGL	AEUC	FA 27/06/1924	14.9	2811	3548	21		
Sioux County	IGGL	AEUC	FA 08/08/1933	20.41	3092	3519	12		
Bereba	VUV	AEUC	FA 27/06/1924	16.84	2903	3437	16		
Andrioniškio (Padvarninkai)	VUV	AEUC	FA 1929	119.7	3023				
Andrioniškio (Padvarninkai)	VUV	AEUC	FA 1929	104.1	3000				
Bialystok	HUB	AHOW	FA 05/10/1827	43.8	2607	3422	24		
Petersburg	TUT	AHOW	FA 05/08/1855	22.5	3261	3462	6	1624	52,955
Luotolax	TUT	AHOW	FA 13/12/1813	19.66	2849	3449	17		
Peña Blanca Spring	UM	AUB	FA 02/08/1946	17.53	2971	2971	0		
Aubres	HUB	AUB	FA 14/09/1836	9.66	2760	3331	17		
Cumberland Falls	IGGL	AUB	FA 09/04/1919	14.9	3041	3725	18	2593	78,862
Norton County	HUB	AUB	FA 18/02/1948	59.5	2861	3839	25		
Karoonda	HUB	CK5	FA 25/11/1930	14.62	2867	4061	29	4607	132,062
Murchison	HUB	CM2	FA 28/09/1969	40.4	2335	3156	26	1021	23,836
Ornans	HUB	CO3.3	FA 11/07/1868	8.05	2597	4237	39		
Renazzo	NHMS	CR2	FA 15/01/1824	22.89	3093	3366	8	11,004	340,370
Allende	TIGT	CV3.2	FA 08/02/1969	21.3	2958	4532	35		
Allende	TIGT	CV3.2	FA 08/02/1969	11.18	2430	5884	59		
Allende	PO	CV3.2	FA 08/02/1969	26.31	2956	3869	24		
Allende	TIGT	CV3.2	FA 08/02/1969	46.77	2960	4032	27		
Allende	PO	CV3.2	FA 08/02/1969	51.5	3121	3787	18		
Allende	PO	CV3.2	FA 08/02/1969	7.85	2804				
Indarch	NHMS	EH4	FA 07/04/1891	41.6	3617	3888	7	24,762	895,749
Pillistfer	HUB	EL6	FA 08/08/1868	17.42	3629			57,483	2,086,157
Tysnes 1	GMO	H4	FA 20/05/1884	38.7	3225	3617	11	6092	196,455
Kashin	VUV	H4	FA 27/02/1918	33.08	3243	3986	19	22,955	744,457
Jilin	NHMS	H5	FA 08/04/1976	73.4	3398	3925	13	21,487	730,156
Hessle	GMO	H5	FA 01/01/1869	23.84	3096			17,381	538,144
Hessle	NHMS	H5	FA 01/01/1869	60.18	3201	3785	15	15,738	503,769
Forest City	IGGL	H5	FA 02/05/1890	149.7	3426			24,642	844,137
Werchne Tschirskaja	NHMS	H5	FA 12/11/1843	43.6	3433	3928	13	21,510	738,438
Pultusk	VUV	H5	FA 30/01/1868	26.5	3487	4206	17	24,579	857,037
Cornesti	EUB	H5	FA 31/03/1875	20.2	3607			22,449	809,754
Madaras	EUB	L3.7	FA 04/09/1852	65	2642			1399	36,957
Nikolskoe	HUB	L4	FA 06/03/1954	39.94	2959	3840	23	6845	202,497
Saratov	VUV	L4	FA 06/09/1918	186.2	3098			7005	217,017
Saratov	PO	L4	FA 06/09/1918	20.2	3061	3885	21	9365	286,626
Hökmark	NHMS	L4	FA 09/06/1954	78.2	3491	3724	6	9551	333,439
Tennasilm	HUB	L4	FA 28/06/1872	45.2	3324	3863	14	5838	194,032
Farmington	UM	L5	FA 25/06/1890	16.24	3383	3314		6234	210,907
Jhung	GMO	L5	FA 06/1873	24.51	3183	3604	12	9844	313,360
Ausson	TUT	L5	FA 09/12/1858	10.2	3290	3923	16	6910	227,365
Homestead	GMO	L5	FA 12/02/1875	79	3511			10,897	382,592
Grefsheim	GMO	L5	FA 25/01/1976	17.95	3520	3387		10,230	360,072
Buschhof	NHMS	L6	FA 02/06/1863	29.3	3368	3617	7	3946	132,890
Bruderheim	UM	L6	FA 04/04/1960	12.51	3381	3381	0	7261	245,515
Girgenti	NHMS	L6	FA 10/02/1853	39	3362	3786	11	9172	308,385
Oteroy 1	GMO	L6	FA 15/10/1928	23.17	3131	3511	11	5755	180,204
Oteroy 2	GMO	L6	FA 15/10/1928	45.33	3309	3656	9	5699	188,559
Žemaitkiemio	VUV	L6	FA 1933	11.56	3211	3853	17	7379	236,939

Table 1. *(Continued)*. New mass-normalized (KM) and volume-normalized (KV) shape-corrected magnetic susceptibility values, bulk (BD) and grain (GD) densities, and porosities (P) of meteorite samples obtained using the mobile laboratory.

Meteorite	Collections	Type	Fall/find (date)	Mass (g)	BD (kg/m^3)	GD (kg/m^3)	P (%)	KM (Osb) (10^{-8} m^3/kg)	KV (Osb) (10^{-6} SI)
Žemaitkiemio	VUV	L6	FA 1933	9.66	3331	3715	10	7813	260,249
Žemaitkiemio	VUV	L6	FA 1933	532.6	3302			9975	329,360
Zabrodje	VUV	L6	FA 22/09/1893	28.1	3306	3958	16	11,585	382,983
Zabrodje	VUV	L6	FA 22/09/1893	18.18	3367	3868	13	11,003	370,444
Zabrodje	IGGL	L6	FA 22/09/1893	32.08	3307	3865	14	11,107	367,317
Ski	GMO	L6	FA 27/12/1848	610.4	3283			8982	294,917
New Concord	VUV	L6	FA 01/05/1860	190.9	3344			9392	314,047
Mocs	EUB	L6	FA 03/02/1882	40.9	3195			5957	190,355
Lundsgard 1	NHMS	L6	FA 03/04/1889	35.1	3311	3052		8060	266,898
Lundsgard 2	NHMS	L6	FA 03/04/1889	66.3	3282			7981	261,957
Oesel	NHMS	L6	FA 11/05/1855	49.6	3179	3906	19	4940	157,059
Bachmut	NHMS	L6	FA 15/02/1814	42.4	3262	3820	15	5275	172,037
Alfianello	GMO	L6	FA 16/02/1883	208.8	2519			9918	249,804
Alfianello 1	NHMS	L6	FA 16/02/1883	129.2	3263			8600	280,584
Aleppo	NHMS	L6	FA 1873	58.7	3298	3473	5	5718	188,571
Žemaitkiemio	VUV	L6	FA 1933	722.2	2951			9941	293,392
Leedey	UM	L6	FA 25/10/1943	8.12	3383	3007		7864	266,056
Ski	GMO	L6	FA 27/12/1848	37.3	3216	3693	13	7758	249,455
Alfianello 2	NHMS	L6	FA 16/02/1883	11.8	3189	3371	5	4065	129,648
Knyahinya	GSHB	L/LL5	FA 09/06/1866	48.2	3324				
Knyahinya	EUB	L/LL5	FA 09/06/1866	39.6	3385			4203	142,245
Knyahinya	EUB	L/LL5	FA 09/06/1866	65.5	3394			5187	176,042
Knyahinya	EUB	L/LL5	FA 09/06/1866	43.3	3331			5054	168,336
Holbrook	VUV	L/LL6	FA 19/07/1912	190.6	3231			5090	164,447
Holbrook	GMO	L/LL6	FA 19/07/1912	15.77	3092	3755	18	4049	125,200
Olivenza	NHMS	LL5	FA 19/06/1924	26.62	3025	3549	15		
Parambu	UM	LL5	FA 24/07/1967	5.29	3306				
Rumuruti	HUB	R3-6	FA 28/01/1934	48.8	3413	3725	8		
Millbillillie	VUV	AEUC	FA 10/1960	31.96	2854				
Pollen	GMO	CM2	FA 06/04/1942	92.9	2266			535	12,120
Mighei	HUB	CM2	FA18/06/1889	18.7	1870	3016	38		
Lance	HUB	CO3.4	FA 23/07/1872	61.9	3346	3537	5	2092	70,002
Lance	NHMS	CO3.4	FA 23/07/1872	14.7	2882	2882	0	1704	49,116
Kaba	GSHB	CV3.0	FA 15/04/1857	3.7	3364			20,625	693,766
Kaba	GSHB	CV3.0	FA 15/04/1857	4.1	6833			24,766	1,692,356
Ekeby	NHMS	H4	FA 05/04/1939	9.92	3100	3968	22	27,137	841,254
Lixna	NHMS	H4	FA 12/07/1820	42.6	3550	3944	10	27,183	965,010
Tysnes 2	GMO	H4	FA 20/05/1884	20.56	3607	3370		12,306	443,872
Wiluna	UM	H5	FA 02/09/1967	13.59	3576	3883	8	28,290	1,011,737
Limerick	NHMS	H5	FA 10/09/1813	15.8	3591	3098		19,713	707,859
Zhovtnevyi	UM	H5	FA 10/10/1938	7.41	3368	3222		13,227	445,501
Juangcheng	PO	H5	FA 15/02/1997	17.93	3898	3815		23,793	927,397
Hedeskoga	NHMS	H5	FA 20/04/1922	31.7	3484	3819	9	27,843	969,930
Pultusk	PO	H5	FA 30/01/1868	110.4	3550			28,354	1,006,510
Pultusk	PO	H5	FA 30/01/1868	22.6	3705	4036	8	19,185	710,796
Charsonville	NHMS	H6	FA 23/10/1810	34.73	3508	3902	10	35,072	1,230,349
Trysil	GMO	L/LL6	FA 21/06/1927	371.1	3389			10,954	371,247
Hallingeberg	NHMS	L3	FA 01/02/1944	15.92	3122	3317	6	4235	132,204
Madaras	NHMS	L3.7	FA 04/09/1852	21.37	3238			5177	167,629
Mount Tazerzait	PO	L5	FA 21/08/1991	12.9	3000	4031	26	6927	207,800
Mbale	PO	L5/6	FA 14/08/1992	15.33	3407	3739	9	9330	317,846
Mocs	EUB	L6	FA 03/02/1882	33.8	3189			8693	277,193
Mocs	GSHB	L6	FA 03/02/1882	14.3	3488			7165	249,909
Bori	NHMS	L6	FA 09/05/1894	48.8	3297	3697	11	7908	260,736

Table 1. *(Continued)*. New mass-normalized (KM) and volume-normalized (KV) shape-corrected magnetic susceptibility values, bulk (BD) and grain (GD) densities, and porosities (P) of meteorite samples obtained using the mobile laboratory.

Meteorite	Collections	Type	Fall/find (date)	Mass (g)	BD (kg/m^3)	GD (kg/m^3)	P (%)	KM (Osb) (10^{-8} m^3/kg)	KV (Osb) (10^{-6} SI)
Marion (Iowa)	GMO	L6	FA 25/02/1847	21.99	3282	3727	12	4841	158,895
Leedey	NHMS	L6	FA 25/11/1943	107.5	3359	3595	7	6676	224,274
Zhigailovka (Kharkov)	TUT	L6 (LL6)	FA 12/10/1787	34.22	3457	4688	26	10,732	370,963
Sena	HMNHB	H4	FA 17/10/1773	94.4	3396			26,076	885,468
Beaver Creek	NHMS	H4	FA 26/05/1893	45.3	3283	3872	15	17,957	589,446
Nuevo Mercurio	UM	H5	FA 15/15/1978	25.1	3218	3922	18	26,408	849,803
Mjelleim	GMO	H5	FA 24/01/1898	99.3	3534			15,837	559,662
Timochin	HMNHB	H5	FA 25/03/1807	107.8	3358			25,425	853,841
Ställdalen	GMO	H5	FA 28/06/1876	115.8	3700			32,449	1,200,513
Ställdalen	NHMS	H5	FA 28/06/1876	53.3	3601	3701	3	36,633	1,319,268
Bialystok	NHMS	AHOW	FA 05/10/1827	43.85	3297	3716	11	7546	248,792
Mocs	HMNHB	L6	FA 03/02/1882	68	3350			6793	227,559
Mocs	HMNHB	L6	FA 03/02/1882	57.2	3467	3667	5	6704	232,393
Mocs	HMNHB	L6	FA 03/02/1882	36.5	3288	3650	10	6680	219,647
Dandapur	HMNHB	L6	FA 03/02/1882	14.6	3395			2932	99,544
Gambat	HMNHB	L6	FA 15/09/1897	90.4	3194			7726	246,782
Aleppo	HMNHB	L6	FA 1873	446	3374			6084	205,245
Marion (Iowa)	NHMS	L6	FA 25/02/1847	58.1	3458	3748	8	4139	143,129
Dhurmsala	HMNHB	LL6	FA 14/07/1860	149.4	3458			34,596	1,196,433
St. Michel	TUT	L6	FA 12/07/1910	62.2	3475	3616	4		
Camel Donga	VUV	AEUC	FI 01/1984	36.62	2839	3130	9	1561	44,326
Camel Donga	PO	AEUC	FI 01/1984	8.3	2594	3609	28		
Reggane	PO	H4	FI 02/04/1989	10.34	3830	3693		12,871	492,903
Cachari	IGGL	AEUC	FI 05/1916	121.9	2916				
Barratta	VUV	L3.8	FI	233.4	3412			13,346	455,400
Waconda	IGGL	L6	FI 1873	88.6	3153			6896	217,431
Estacado	PO	H6	FI 1883	8.8	3259	3826	15	28,214	919,560
Estacado	GMO	H6	FI 1883	51.76		3671			
Beenham	UM	L5	FI 1937	8	3333	3200		5773	192,442
Mount Egerton	HUB	MES (AUB)	FI 1941	14.76	3514	3433		1625	57,107
Mulberry Draw	UM	L5	FI 1963	23.74	3391	3441	1	3827	129,806
Tsarev	PO	L5	FI 1968	48.4	3667	3667	0	6456	236,712
ALH 76001	GMO	L6	FI 1976	116.7	3278			6343	207,932
Julesburg	HUB	L3.6	FI 1983	33.98	3503	3818	8	8659	303,317
Owasco	VUV	L6	FI 1984	18.64	3159	3452	8		
Oliver	UM	L6	FI 1984	12.54	3389	3389	0	3018	102,287
Acfer 90087	UM	CR2	FI 1990	23.7	3292	4086	19	10,830	356,486
Hughes 021	HUB	L3.6	FI 1991	4.89	3493	3944	11		
DaG 067	UM	CO3	FI 1995	31.88	3321	3542	6	2753	91,420
DaG 391	UM	AEUC	FI 1997	18.09	2966	3289	10		
DaG 380	UM	AEUC	FI 1997	18.22	3037	3644	17		
Sahara 97193	HUB	L3.9	FI 1997	28.5	3701	3851	4	4402	162,926
Dhofar 055	UM	AEUC	FI 1999	13.62	2961	3322	11		
SaU 281	HUB	EH3	FI 2001	12.96	2817	3600	22	6553	184,611
Svartekari	GMO	H5	FI 2001	711.5	3552			39,344	1,397,571
Nova 004	UM	H5	FI 2002	42.06	3448	3894	11	27,167	936,606
NWA 3094	HUB	L6 imp. melted	FI 2003	31.7	3446	3774	9	13,235	456,035
NWA 3080	HUB	L6 imp. melted	FI 2003	18.5	3627	3627	0	11,711	424,796
NWA 3050	HUB	L6 imp. melted	FI 2003	14.1	3439	3811	10	5607	192,823

Table 1. *(Continued)*. New mass-normalized (KM) and volume-normalized (KV) shape-corrected magnetic susceptibility values, bulk (BD) and grain (GD) densities, and porosities (P) of meteorite samples obtained using the mobile laboratory.

Meteorite	Collections	Type	Fall/find (date)	Mass (g)	BD (kg/m^3)	GD (kg/m^3)	P (%)	KM (Osb) (10^{-8} m^3/kg)	KV (Osb) (10^{-6} SI)
NWA 3057	HUB	L6 imp. melted	FI 2003	26.5	3581	3897	8	17,587	629,817
Hanno 04 (NWA)	HUB	L4 imp. melted	FI 2004	13.59	3398	3883	13	8334	283,160
Fortuna	HUB	AWIN	FI 27/05/1998	9.52	3662	4533	19	20,682	757,272
Dhofar 125	HUB	ACAP	FI 2000	29.04	3585	3676	2	9334	334,645
Kenna	HUB	AURE	FI 1972	31.3	4118	3598		3899	160,568
Hammadah al Hamra 126	HUB	AURE	FI 1972	21.19	3451	3418		3806	131,364

Legend to the collections and meteorite classes: EUB-Eötvös. University, Budapest, Hungary. GMO-Geological Museum, Oslo, Norway. HMNHB-Hungarian Museum of Natural History, Budapest, Hungary. GSHB-Geological Survey of Hungary, Budapest, Hungary. HUB-Humboldt University, Berlin, Germany. IGGL-Institute. of Geology and Geography of Lithuania, Vilnius, Lithuania. NHMS-Natural History Museum, Stockholm, Sweden. PO-Planetarium Olsztyn, Poland. TIGT-Tallinn Institute of Geology, Tallinn, Estonia. TUT-Tartu University, Tartu, Estonia. UM-Planetary Institute, University of Münster, Münster, Germany. VUV-Vilnius University, Vilnius, Lithuania. ACA-Acapulcoite. AEUC-Eucrite. AHOW-Howardite. AUB-Aubrites. AURE-Ureilites. CX-Carbonaceous chondrites. H, L, LL-Ordinary chondrites. MES-Mesosiderites.

according to the dipole rules will generate data sets containing induced magnetization that allow an estimate of magnetic susceptibility. However, the solar wind interaction with the surface is a complex process and has to be considered during such an estimate of magnetic susceptibility (Omidi et al. 2002). In the case the plasma carrying the external magnetic field H is homogenous during the measurement period (couple of orbits), the resulting magnetic induction B measured on orbit of the asteroid is

$$\begin{aligned} B &= \mu H \\ B &= \mu_0 \mu_r H \\ B &= \mu_0 (1+\kappa) H \\ B &= \mu_0 H + \mu_0 \kappa H \\ B &= \mu_0 (H + M) \\ B &= B_s + B_a \end{aligned} \tag{4}$$

where μ is permeability, μ_o is permeability of vacuum, μ_r is relative permeability, κ is volume normalized magnetic susceptibility, M is magnetization induced by H, B_s is an induction from the Sun and B_a is an induction from the asteroid.

B_a propagates as magnetic dipolar field according to:

$$B_a = \frac{\mu_0}{4\pi}\frac{m}{r^3}\sqrt{1+3\sin^2\alpha}\,, \tag{5}$$

where m is a magnetic moment of the asteroid, r is a distance form the center of the asteroid, and α is the magnetic latitude of the dipole.

Dipole Equation 5 can be detected as the difference between the asteroid induction $B_a(90^\circ) = \frac{\mu_0}{2\pi}\frac{m}{r^3}$ over the magnetic pole (case A in Fig. 3) and asteroid induction $B_a(0^\circ) = -\frac{\mu_0}{4\pi}\frac{m}{r^3}$ over the magnetic equator (case B in Fig. 3, note the negative sign reflecting the opposing direction in respect to inducing field B_s).

This difference due to dipolar character of the induced field suggests a scheme for detection of an induced component on board of the spacecraft. The data has to be transformed into a coordinate system such that the vertical direction is parallel to spacecraft-asteroid direction. If the magnetic field B_A is parallel to spacecraft-asteroid direction, we have the case A in Fig. 3. If the magnetic field B_B is perpendicular, we have the case B in Fig. 3. The difference between these two cases δB can be expressed as following:

$$\begin{aligned} \delta B &= B_A - B_B \\ \delta B &= B_s + B_a(90^\circ) - B_s - B_a(0^\circ) \\ \delta B &= B_a(90^\circ) - B_a(0^\circ) \\ \delta B &= \frac{\mu_0}{2\pi}\frac{H}{r^3} + \frac{\mu_0}{4\pi}\frac{m}{r^3} \\ \delta B &= \frac{3\mu_0}{4\pi}\frac{m}{r^3} \end{aligned} \tag{6}$$

where m is the magnetic moment for which we have:

$$\begin{aligned} m &= M V_a \\ m &= \kappa H V_a \end{aligned} \tag{7}$$

where M is asteroid's magnetization, κ is bulk susceptibility (asteroid volume (V_a) normalized) and H is magnetic field, so we have:

$$\begin{aligned} \delta B &= \frac{3\mu_0}{4\pi}\frac{\kappa H}{r^3} V_a \\ \delta B &= \frac{3}{4\pi r^3}\kappa V_a V B_s \end{aligned} \,. \tag{8}$$

where B_s is the solar induction. Equation 8 allows detection of

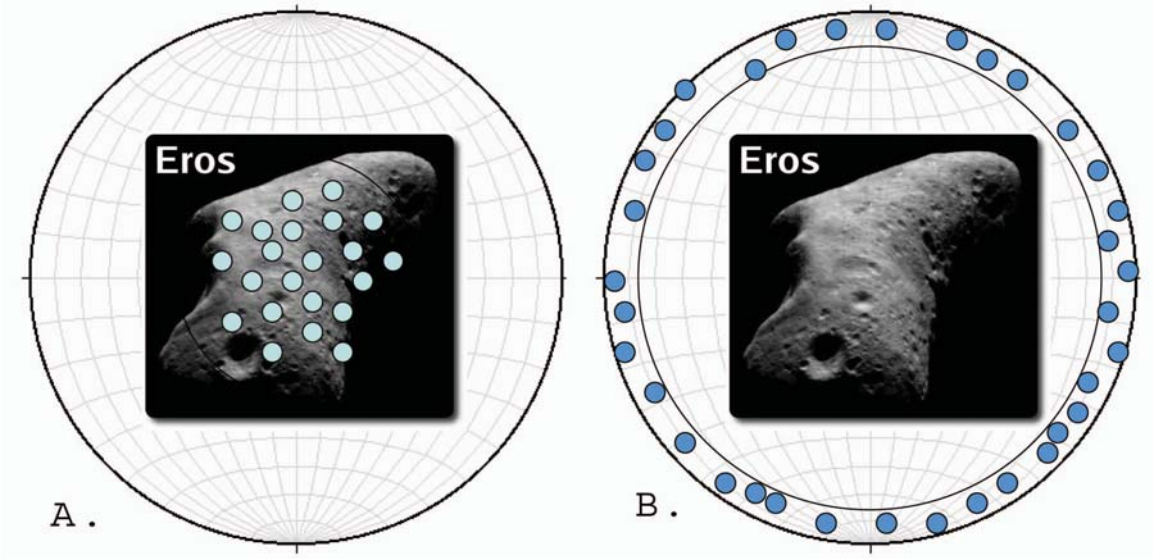

Fig. 3. Green and blue circles indicate magnetic orientations of the vector magnetic data during the orbiting of the asteroid. Background image (Eros asteroid) is shown just for concept visualization. a) Magnetic field directions (green circles) is directed towards the asteroid at the magnetometer location. b) Blue circles indicate magnetic vector directions of the magnetic field pointing 90 degrees away from the asteroid direction.

susceptibility of the entire asteroid from any data set satisfying the case A and B (Fig. 3). For B_s we can use an average from values B_A and B_B:

$$B_{av} = \frac{B_A - B_B}{2}$$

$$B_{av} = B_s + \frac{B_a(90°) + B_a(0°)}{2}$$

$$B_{av} = B_s + \frac{\mu_0}{4\pi}\frac{m}{r^3}$$

$$B_{av} = B_s + \frac{\mu_0 H}{4\pi r^3}\kappa V_a \qquad (9)$$

$$B_{av} = B_s + \frac{B_s}{4\pi r^3}\kappa V_a$$

$$B_{av} = B_s\left(1 + \frac{\kappa V_a}{4\pi r^3}\right)$$

$$B_{av} \sim B_s$$

because the term $\frac{\kappa V_a}{4\pi r^3} = \kappa\frac{V_a}{3V_r} < \kappa\frac{1}{100} << 1$ for r > 1.5 ~~ra~~ (radius of an asteroid) and susceptibility κ even ≤ 1.
Finally we obtain:

$$\kappa = \frac{8\pi r^3}{3V_a}\frac{\delta B}{(B_A + B_B)} \qquad (10)$$

Equation 10 can be used to estimate the apparent bulk susceptibility κ_{bulk} of an asteroid.

The advantage of this method is that the magnetic susceptibility of the whole asteroid is determined. This gives us the susceptibility value representative for the whole asteroidal volume and free of surface related space weathering ~~a~~affects. However, compared to the surface or sample return measurements, the sensitivity and precision of this method is low.

A typical IMF in the asteroid belt is ~~about a~~ nT, but can reach larger amplitudes during the periods of the high solar activity, giving better signal to noise ratio. The induced magnetic field decays with power of three of the distance from the asteroid, thus requiring close orbits.

The detection limit and desired magnetometer sensitivity depends on two main factors: the strength of the IMF field and the orbiting distance. To estimate the detection limit we will use in our calculation a spherical asteroid, radius of the orbit two times larger than the radius of the asteroid $r = 2r_a$ (to meet the condition in Equation 9) and IMF strength 10 nT. Then by using the approximation from Equation 9:

$$B_s \sim B_{av} = \frac{B_A + B_B}{2}$$

and

$$V_a = \frac{4}{3}\pi r_a^3$$

the Equation 10 will transfer to

$$\kappa = \frac{r^3}{r_a^3}\frac{2\delta B}{B_s} = \frac{8r_a^3}{r_a^3}\frac{2\delta B}{B_s} = \frac{16\delta B}{B_s} \qquad (11)$$

For an asteroid with CH, E, or H composition equivalent

(κ_{bulk} ~1 SI) and IMF strength 10 nT, the measured variation due to the induced effect will be ~0.6 nT and for CR, H or Ureilite composition equivalent (κ_{bulk} ~0.1 SI) the measured variation due to the induced effect will be ~0.6 nT.

Thus in the case of strongly magnetic stony asteroids or metallic objects, the detection of magnetic susceptibility (and thus estimate of the iron content) is possible using currently available magnetometers with a 10^{-1} nT–10^{-2} nT resolution. In the case of stony asteroids with a lower magnetic content, the development of more sensitive instrumentation or use of other method (as described further) is needed.

Another problem is related to the time variation of the IMF. This method assumes IMF to be constant through the measurement period. Thus, the measurement must be performed during the relatively stable IMF periods or the second spacecraft far from an asteroid is required to monitor the variations of undisturbed IMF.

Active Detection of Asteroidal Magnetic Susceptibility using a Surface Probe (AC Coil) Attached to a Lander

In the case surface landing is part of a mission to an asteroid, a simple AC magnetic coil surface probe can be used to measure magnetic susceptibility. This concept is described in detail in Rochette et al. (2004). The advantage of this method is that the signal of the material induced by the coil is much stronger compared with the IMF interactions. The depth penetration of the coil signal depends on its diameter (roughly equal to the coil diameter), and usually the flat surface is required for best precision.

However, the effect of the space weathering on the magnetic properties of the asteroidal surface is not well known. In the case of a solid rocky surface of an asteroid, the combination of the surface susceptibility probe with the device similar to RAT (Rock Abrasion Tool) used on Mars Exploration Rovers could provide the magnetic susceptibility of the unweathered asteroidal material. Other disadvantage is that the surface material of the asteroid can be modified or contaminated through collisional impact processes. For these reasons the magnetic susceptibility determined by the surface probe may not be representative for the whole asteroid.

Direct Measurement of the Asteroidal Sample Return

In the case when a sample of an asteroid is delivered to terrestrial laboratories, magnetic susceptibility can be measured using sensitive and well-calibrated laboratory instrumentation. However, the expected sample size of the sample return for the ongoing (Hayabusa) or planned mission is typically very small (~mg) and may also be influenced by the effects described in the previous case. Thus, it may not be representative for the whole asteroid either.

MASS VERSUS BULK SUSCEPTIBILITY

The bulk volume V_B, mass m, bulk density ρ_B, and shape are among the primary asteroid parameters determined during the orbital phase of a remote sensing mission to an asteroid. the knowledge of both bulk volume and mass of the asteroid allows the determination of both bulk (volume-normalized) and mass-normalized susceptibilities of the asteroid. The relation between mass and bulk susceptibilities is expressed by Equation 11:

$$\kappa_{mass} = \frac{\kappa_{bulk}}{\rho_B} \tag{11}$$

The bulk susceptibility is essential to calculate the shape correction of the measured (apparent) susceptibility using the demagnetizing factor and Equation 1. However the bulk volume V_B of the asteroid may vary according to the porosity of the asteroid. An asteroid of the same mass and grain volume V_G (and thus same amount of magnetic compounds), but higher pore volume V_P, will have larger bulk volume V_B resulting in a lower bulk susceptibility. Thus bulk susceptibility is not suitable for magnetic classification purposes.

However, the mass m and grain volume V_G remains the same and thus susceptibility normalized by mass or by grain volume will remain independent of the change in porosity. For this reason, it is suitable to first perform the shape correction of the apparent bulk susceptibility and then normalize the true bulk susceptibility by mass or grain volume in order to minimize the porosity effect. Then the mass (or grain volume normalized) true susceptibility can be directly compared to those of meteorites.

CONCLUSIONS

Determination of the asteroidal susceptibility is not a trivial task, but is possible. Each of three methods described has its own advantages and disadvantages. The induced effects due to the IMF interactions can provide the susceptibility representative for the whole asteroid. However the precision of this method is lower and thus is suitable for the highly susceptible bodies only. The use of surface probe or the laboratory measurement of a returned sample can provide more reliable values and can bring results also for materials of lower susceptibility (e.g., achondrites). However, these methods bring the information from the asteroid surface only and thus may not be representative for the whole asteroid.

Once magnetic susceptibility is successfully determined, the amount and nature of the magnetic minerals can be inferred. Based on the susceptibility, asteroids can be classified in similar ways as meteorites are. We expect the distribution of magnetic susceptibility among various asteroid compositions to reflect the distribution of their meteorite equivalents.

Similar to meteorites, the range of the susceptibilities of some asteroid classes may overlap. But additionally to reflectance spectroscopy and other chemical and mineralogical remote sensing methods, the magnetic classification may refine the match among meteorite equivalent candidates.

Thus, we propose a stepwise concept of asteroid characterization and classification. First, the spectral class will be determined based on reflectance spectroscopy classification and the corresponding meteorite clan will be determined. Second, based on the asteroid magnetic susceptibility and chemical and mineralogical information from the instruments on board the space probe, the matching meteorite group will be distinguished. This multidisciplinary approach will help us get the most precise link among asteroids and meteorites.

Once the meteorite equivalent will be distinguished, other physical parameters (bulk and grain density, porosity) of the asteroid and corresponding meteorite group in the database can be compared to obtain more information about the internal structure asteroid. For example, by comparing the bulk and grain densities of the asteroids and meteorites, the amount of micro- and macro-porosity can be estimated. The micro-porosity is assumed to be similar among asteroids and related meteorites ~~due to~~ the small (submillimeter) ~~pore size~~. This approach was applied in past studies to determine amount of the micro- and macro-porosity and the internal structure (rubble pile versus onion skinned) of asteroids Eros (Wilkinson et al. 2000) and Itokawa (Abe et al. 2006). The macro-porosity observed on asteroids is not preserved in meteorites because of the large-scale cracks/faults building the pore space. In this case, the meteorites are simply too small to preserve those large-scale cracks.

Acknowledgments–This work was financially supported by Academy of Finland project, Sohlberg Delegation research grant, NSF EAR-0609609, and Väisälän Foundation travel grant. We would like to thank V. Kohout for his help with the meteorite measurements and M. Lehtinen (Geological Museum, University of Helsinki, Finland), H. Pärnaste (Geological Survey of Estonia, Tallinn), J. Plado (Tartu University, Estonia), B. Poshkiene (Geology and Mineralogy Museum, Vilnius, Lithuania), E. Rudnickaite and G. Motuza (Vilnius University, Lithuania), J. Biala and J. Szubiakowski (Planetarium and Observatory Olsztyn, Poland), O. Kákay-Szabó (Geological Institute of Hungary, Budapest, Hungary), T. Weiszburg (Eötvös L. University, Budapest, Hungary), A. Embey-Isztin (Museum of Natural History, Budapest, Hungary), M. Bukovanská (National Museum, Prague, Czech Republic), A. Martaus and B. Kratochvíl (Chemical University, Prague, Czech Republic), A. Greshake (Humboldt University of Berlin, Germany), A. Bischoff (University of Münster, Germany), G. Raade (University of Oslo, Norway), J. O. Nyström (Swedish Museum of Natural History, Stockholm, Sweden) for their cooperation and help in providing access to the meteorite collections.

Editorial Handling—Dr. Louise Prockter

REFERENCES

Abe S., Mukai T., Hirata N., Barnouin-Jha O. S., Cheng A. F., Demura H., Gaskell R. W., Hashimoto T., Hiraoka K., Honda T., Kubota T., Matsuoka M., Mizuno T., Nakamura R., Scheeres D. J., and Yoshikawa M. 2006. Mass and local topography measurements of Itokawa by Hayabusa. *Science* 312:1344–1347.

Britt D. T. and Consolmagno G. J. 2001. Stony meteorite porosities and densities: A review of the data through. *Meteorites & Planetary Science* 38:1161–1180.

Bus S. J. and Binzel R. P. 2002. Phase II of the small main-belt asteroid spectroscopic survey—A feature-based taxonomy. *Icarus* 158:146–177.

Consolmagno G. J. and Britt D. T. 1998. The density and porosity of meteorites from the Vatican collection. *Meteoritics & Planetary Science* 33:1231–1241, 1533–1546.

Kletetschka G., Adachi T., and Mikula V., Electromagnetic spacecraft used for magnetic navigation within asteroid belt, mining concepts and asteroid magnetic classification ~~(abstract #1093)~~. 38th Lunar and Pla[illegible] Science Conference ~~CD-ROM~~.

Kohout T., Elbra T., Pesonen L. J. Schnabl P., and Slechta S. 2006. Applications of the meteorite physical properties data obtained using mobile laboratory facility (abstract). *Meteoritics & Planetary Science* 41:A98.

Kukkonen I. T. and Pesonen L. J., 1983. Classification of meteorites by petrophysical methods. *Bulletin of the Geological Society of Finland* 55:157–177.

Omidi N., Blanco-Cano X., Russell C. T., Karimabadi H., and Acuña M. 2002. Hybrid simulations of solar wind interaction with magnetized asteroids: General characteristics, *Journal of Geophysical Research* 107:1487, doi:10.1029/2002JA009441.

Osborn J A. 1945. Demagnetizing factors of the general ellipsoid. *Physical Review* 67:351–357.

Rochette P., Gattacceca J., Bonal L., Bourot-Denise M., and Chevrier V. Clerc J.-P., Consolmagno G., Folco L., Gounelle M., Kohout T., Pesonen L., Quirico E., Sagnotti L., and Skripnik A. 2008. Magnetic classification of stony meteorites: 2. Non-ordinary chondrites. *Meteoritics & Planetary Science* 43:959–980.

Rochette P., Gattacceca J., Menvielle M., Eisenlohr P., and Chevrier V. 2004. Interest and design of magnetic properties measurements on planetary and asteroidal landers. *Planetary and Space Science* 52:987–995.

Rochette P., Sagnotti L., Bourot-Denise M., Consolmagno G., Folco L., Gattacceca J., Osete M. L., and Pesonen L. 2003. Magnetic classification of stony meteorites: 1. Ordinary chondrites. *Meteoritics & Planetary Science* 38:251–268.

Rochette P., Sagnotti L., Consolmagno G., Folco L., Maras A., Panzarino F., Pesonen L., Serra R., and Terho M. 2001. A magnetic susceptibility database for stony meteorites. *Quaderni di Geofisica* 18:30.

Terho M., Pesonen L. J., and Kukkonen I. T. 1993a. Physical properties of 368 meteorites: Implications for meteorite magnetism and planetary geophysics. *Proceedings of the NIPR Symposium on Antarctic Meteorites* 6:601–416.

Terho M., Pesonen L. J., Kukkonen I. T., and Bukovanská M. 1993b. The petrophysical classification of meteorites. *Studia Geophysica et Geodetica* 37:65–82.

Tholen D. J. 1984. *Asteroid taxonomy from cluster analysis of photometry*. Tucson: The University of Arizona. X p.

Wasilewski P. J., Acuña M. H., and Kletetschka G. 2002. 433 Eros: Problems with the meteorite magnetism record in attempting an asteroid match. *Meteoritics & Planetary Science* 37:937–950.

Wasson J. T. and Wetherill G. W. 1979. In *Asteroids*, edited by Gehrels T. and Matthews M. S. Tucson: The University of Arizona Press. pp. 926–974.

Wilkinson S. L., Robinson M. S., Thomas P. C., Veverka J., McCoy T. J., Murchie S. L., Prockter L. M., and Yeomans D. K. 2002. An estimate of Eros's porosity and implications for internal structure. *Icarus* 155:94–103.

Wilkinson S. L., McCoy T. J., McCamant J. E., Robinson M. S., and Britt D. T. 2003. Porosity and density of ordinary chondrites: Clues to the formation of friable and porous ordinary chondrites. *Meteoritics & Planetary Science* 38:1533–1546.